

VARACTOR LOADED TUNABLE PRINTED PIFA

J. Liang and H. Y. D. Yang

Department of Electrical and Computer Engineering
University of Illinois at Chicago
851 S Morgan Street, M/C 154, Chicago, IL 60607, USA

Abstract—Varactor tuned printed planar inverted-F antennas (PIFA) are investigated. The low-profile printed antennas are fabricated together with the layouts of its DC control circuits and other RF/base-band circuit footprints. A surface mounted (SMT) varactor is applied as a frequency-tuning element at the middle of the long radiating arm in PIFA. Passive lumped DC bias circuits are implemented with good isolation. Both single and dual-band varactor tuned PIFA antennas are investigated. For a single-band PIFA, prototype designs show the in-band frequency (return loss is <10 dB) is tunable from 1.6 GHz to 2.3 GHz when the bias voltage varies from 0 V to 9.5 V. Measured results show about 70~75% efficiency and 2~3 dB maximum gain. For a dual band PIFA with two varactor loadings, both the 800~900 MHz and 1.7~2.2 GHz bands are tuned individually by a varactor. By varying low-band capacitance, the operation frequency is tuned from 780 MHz to 1020 MHz, with little change on the higher frequency band. By varying high-band capacitance, the operation frequency is tuned from 1700 MHz to 2140 MHz, with little change on the lower frequency. Measurement shows antenna radiation efficiencies within operation bands are about 55% at the low band and about 45% at the high band. The proposed frequency reconfigurable antennas could be useful for personal mobile terminal applications.

1. INTRODUCTION

With the rapid growth of wireless markets (mobile communication, WLAN networking, GPS services and RFID applications), in recent years, RF engineers are facing continuing challenges of small-volume, multi-bands, wide bandwidth, power efficient, and low-cost system

Corresponding author: H. Y. D. Yang (hyang@ece.uic.edu).

designs. A low-profile, small size antenna integrated into RF front-ends with sufficient bandwidth is essential in wireless systems. Printed antenna is useful due to its low profile, low fabrication cost, and simple feeding structures. The inherent drawback is the narrow bandwidth for a small antenna size. The demand of a smaller antenna size often conflicts with the desired wide band or multi-band applications.

Reconfigurable or tunable antennas provide a possible solution and have attracted significant research efforts [1–4]. Rather than supporting wide-band or multi-band operations simultaneously, reconfigurable antennas are manipulated to hop over different bands dynamically. Such an antenna would not cover all bands at the same time, but it provides a narrow instant bandwidth that is selectable dynamically.

Since antenna radiation characteristics, including resonant frequency and radiation patterns are determined mostly by its shape and size, varying its geometry mechanically provides an intuitive method to reconfigure its radiation properties. MEMS techniques integrate electrical and mechanical functions in a single component using microfabrication or micromachining technology, and can be realized with present semiconductor integrated circuit processing [5–7]. Hence, MEMS based reconfigurable antennas had been widely investigated [8–12]. A MEMS switch changes dynamically the antenna length and enables dual or multi-band applications.

Antenna reconfiguration can also be designed using electronics switch such as PIN diodes, which are commonly used in modern communications and radar applications. Planar microstrip antennas using PIN diode switching for reconfiguration had also been investigated [13–16].

A PIFA is similar to a freestanding quarter-wave monopole above a ground plane, but with an inductive tuning stub in parallel with the capacitive radiating arm. Multiband PIFA for mobile applications were proposed [17, 18]. Frequency reconfiguration using diode switches [18–22] or MEMS switches [23–25] had been investigated quite extensively for several versions of free-standing PIFA. Recently, printed PIFA antennas were used extensively in portable wireless communication due to a much wider bandwidth (20~30%) and the small size by removing the ground backing underneath the wire antenna [26]. In this paper, first a varactor-loaded printed PIFA is investigated. The PIFA is integrated on a circuit board and a varactor is mounted in the middle of its capacitive radiating arm. DC control circuits that provide the bias for the varactor, antenna layouts, and varactor specifications are detailed. Antenna prototypes with tuning range from 1.6 GHz to 2.3 GHz (0 V to 9.5 V biasing) are designed, fabricated, and tested.

The results of return loss, efficiency, gain, and radiation patterns are discussed.

In addition to the DCS/PCS/UMTS new standards that utilize the 1.7~2.2 GHz bands, the 3G wireless terminals also include 800 MHz~900 MHz bands. Therefore, it is desirable that the frequency-reconfigurable antennas cover 3G low bands and high bands simultaneously. In this paper, a double varactor-loaded dual frequency-band tunable stacked inverted-F antenna is also proposed to solve this problem.

2. A CAPACITOR-LOADED PRINTED PIFA

The printed PIFA is modeled and designed with HFSS simulation and fabricated on a double-side rigid FR4 PCB 50 mm wide, 80 mm long, and 1.575 mm (62 mils) thick. The layout and prototype is shown in Fig. 1. The RF ground plane is cut off with 15 mm clearance below the antenna layout. Antenna is fed by a 50 Ohm microstrip line (3 mm wide) with a SMA connector at the edge.

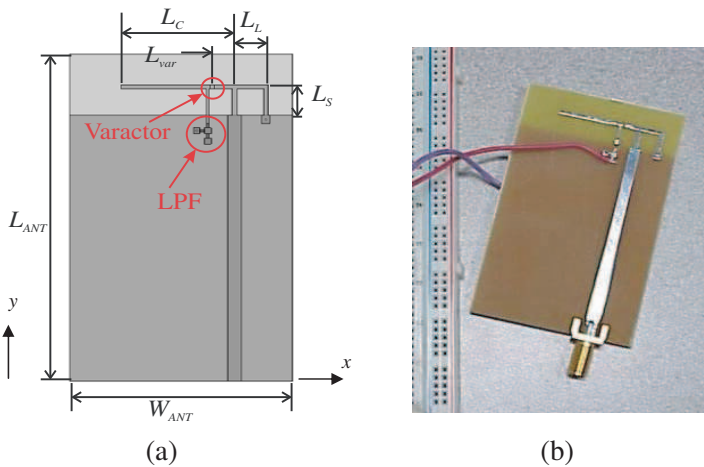


Figure 1. (a) Antenna layout and the parameters. (b) Printed PIFA prototype with a lump ceramic varactor loading.

The frequency tunability of this PIFA is investigated first by loading a lump ceramic capacitor instead of a varactor diode. Hence, the DC bias circuit parasitic effects are excluded. The intent is to determine how the loaded capacitor could affect the antenna performance and its optimized location on the antenna radiation arm. First, actual prototype in Fig. 1 is fabricated and tested except without

the bias circuit. Several different RF capacitors available commercially are mounted and tested, one at a time.

The antenna could be for DCS1800, PCS1900, and UMTS applications covering the frequency from 1.6 to 2.3 GHz. The higher-band corresponds to a lower capacitance. In extreme case of an open circuit ($C = 0$ pF), the arm will be effectively smallest in length and the PIFA will be for the highest band (2.3 GHz). Based on the simulation results from HFSS, the PIFA dimensions are $L_c = 25$ mm, $L_L = 7$ mm, $L_S = 7$ mm, and trace width is 1 mm. Several capacitor positions relative to the vertical feed arm L_{var} are simulated to determine the frequency tunability. The return losses for $L_{\text{var}} = 5$ mm and $L_{\text{var}} = 15$ mm are shown in Fig. 2. Four different lump capacitance values ($C_{\text{var}} = 0.5, 1.5, 2.4,$ and 3.6 pF) are chosen for investigation.

It is found that with a smaller distance between capacitor and the feed point, the wider tunability range of the antenna can be achieved. In details, for the $L_{\text{var}} = 5$ mm case, the antenna dynamic frequency bands are from 1.69~1.89 GHz at 3.6 pF to 2.09~2.31 GHz at 0.5 pF. Hence, the static band-width for this case is around 11%, while the dynamic band-width is about 31.0%. In contrast, when the varactor is moved to $L_{\text{var}} = 15$ mm, its dynamic operation bands are from 1.60~1.83 GHz at 3.6 pF to 1.82~2.03 GHz at 0.5 pF. The static band-width for this case is also around 11%, but its dynamic operation band is about 23.7%. Basically, the highest useful band corresponds to the smallest capacitance case where the arm, in effect, breaks into two and the PIFA looks smaller with a higher resonant frequency. One can also observe that by increasing L_{var} , the tunable frequency range scales down. For the extreme case, when the capacitor is located at the tip of the radiation arm, it will have little effect on the electrical length and radiation. In other words, as the capacitor location moves close to the open end, it is less effective in varying the antenna length and the frequency tuning range decreases. However, L_{var} should not be too small so that the bias circuit will interfere with the microstrip feed. $L_{\text{var}} = 5$ mm is a sensible but not a unique choice that provides useful tuning range.

Capacitor loaded PIFA with $L_{\text{var}} = 5$ mm was built and tested. RF capacitors of $C_{\text{var}} = 0.5, 1.5, 2.4$ and 3.6 pF are soldered into the gap of the PIFA radiation arm, one at a time. The return loss based on vector network analyzer measurements is shown in Fig. 3. It is observed that the PIFA dynamic bands (-10 dB return loss band) can be tuned from 1.692~1.914 GHz at 3.6 pF to 2.076~2.322 GHz at 0.5 pF. Therefore, the simulation results match very well with the actual prototype measurement for the port impedance in the direct capacitor loading case.

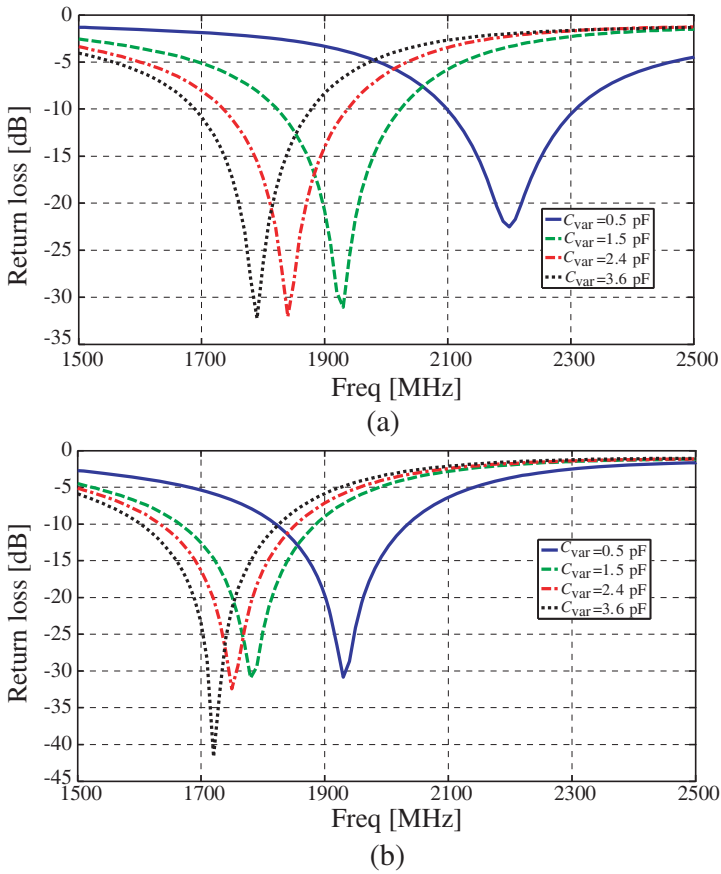


Figure 2. Return loss of the capacitor loaded PIFA based on HFSS simulation: (a) $L_{var} = 5$ mm; (b) $L_{var} = 15$ mm.

Furthermore, antenna radiation patterns in the three principle planes are obtained by both HFSS simulations and anechoic chamber measurements. The radiation patterns are found similar to a regular printed PIFA without any loading. The resonant frequency, instant bandwidth, maximum gain, and antenna efficiency are summarized in Table 1. Good agreements between simulation and measurement are found. However, since the EM simulations did not account the lump ceramic capacitor non-idea parasitic package and bonding effects in addition to the fabrication and testing accuracy, the chamber measurements and the EM simulations have discrepancy in efficiency (75~80% by measurement and 94~96% by simulation) and maximum

gain (1.9~2.8 dBi by measurement and 2.8~2.9 dBi by simulation). Over 75% efficiency within the instant bandwidth over the tuning range is quite reasonable for a multi-band-band antenna.

Table 1. Simulated and measured antenna parameters of capacitor-loaded PIFA.

	Loading Cap. [pF]	Res. Freq [GHz]	Instant BW [%]	Max Gain [dBi]	Efficiency [%]
Sim.	0.5	2.20	9.5	2.92	96.0
	1.5	1.93	10.4	2.67	93.9
	2.4	1.84	11.4	2.82	94.3
	3.6	1.79	10.6	2.83	94.1
Meas.	0.5	2.17	11.2	2.84	80.4
	1.5	1.93	12.5	2.86	80.6
	2.4	1.85	10.2	2.24	75.9
	3.6	1.79	12.6	1.93	75.8

3. VARACTOR AND THE DC BIAS CIRCUITS

Having shown the feasibility of frequency tuning using loaded capacitors, a varactor loaded printed PIFA with a DC bias circuit is explored. The varactor used in this work is Panasonic MA27V19 silicon epitaxial SMT planar type variable capacitance diodes, which

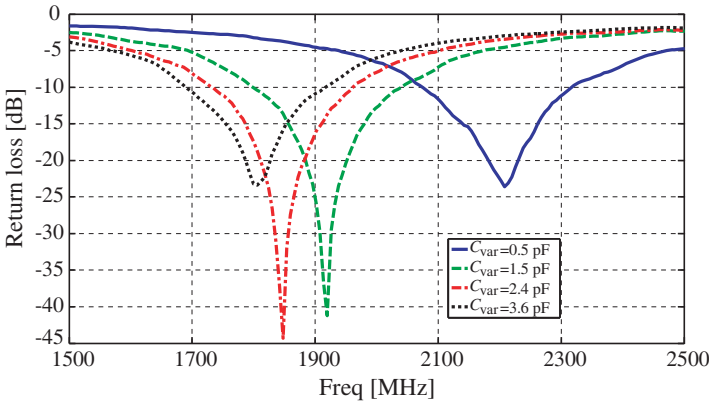


Figure 3. Measured return loss of the capacitor loaded PIFA with $L_{\text{var}} = 5$ mm (simulation is shown in Fig. 2(a)).

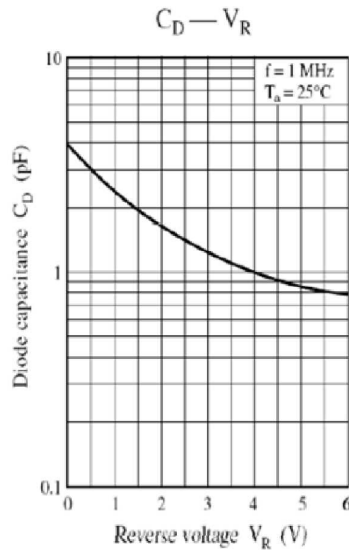


Figure 4. Panasonic MA27V19 varactor junction capacitance versus reverse bias voltage.

is small and commercially available off the shelf. The diode junction capacitance as a function of reverse bias voltage is shown in Fig. 4 according to [27]. It is observed that the maximum varactor capacitance is about 3.9 pF and pretty much saturated at 6 V (0.8 pF). It is found that at 9.5 V, the capacitance is about 0.5 pF, which is pretty much the lowest value one can get. Practically, 0.5 pF or 0.8 pF makes little difference in radiation characteristics. From the results in Fig. 3, the tuning range for PIFA using this varactor should provide over 30% tunable bandwidth at 2 GHz.

Both lumped and distributed DC bias circuits are possible to control the tuning varactor DC voltage. Generally speaking, when the operation frequency is above 3 GHz, the parasitic package effects and self resonances of the lump components are becoming more and more significant. Then, the distributed passive transmission line equivalent designs such as the open radial stub bias cascading with a quarter-wave high-impedance transmission line can be used [28]. For the present design at around 2 GHz, a lump low-pass filter (LPF) using high-performance ceramic lump capacitors and inductors is sufficient for RF isolation.

The LPF circuit shown in Fig. 5(a) comprises two series RF choke inductors and a shunt by-pass capacitor, which are used to decouple the RF current to the DC voltage source. The Johanson Technology

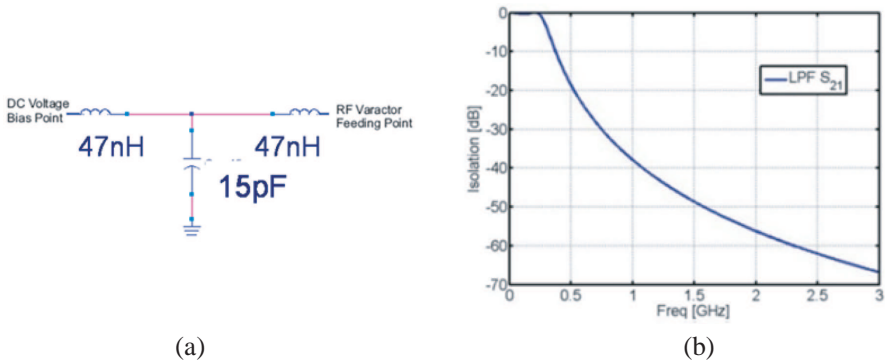


Figure 5. Lump LPF for DC bias circuit and its RF isolation.

0402 series ceramic SMT prototype kits are used, with LPF inductance 47nH and capacitance 15pF. The circuit simulation of the LPF is shown in Fig. 5(b). The isolation between the RF varactor bias point and DC voltage feed point is lower than -18.65 dB at 500 MHz, and even lower than -48.69 dB at 1.5 GHz. Hence, it is shown that the high-frequency signals are isolated effectively by the lump LPF circuit.

4. A VARACTOR-LOADED PRINTED PIFA

The actual varactor loaded printed PIFA prototype together with the DC bias circuit is shown in Fig. 1 and the varactor and bias circuit were discussed in the last section. The SMT varactor is located at a small gap on the long radiation arm (Fig. 1). Hence, the radiation current is controllable as the varactor capacitance changes. The bias trace is right next to the SMT varactor, and extended back to the RF ground plane. The DC bias circuit is also shown where DC voltage is fed to a lump SMT RF low-pass filter. Furthermore, since the PIFA is DC short to the ground through the inductive arm, the negative terminal of DC voltage across the varactor is automatically connected to the RF ground plane on the backside.

The antenna characteristics are investigated first by using 2-port HFSS simulation with voltage varying from 0 to 9.5 V (the junction capacitance decreasing from 3.9 pF to 0.5 pF). One port is the antenna input from microstrip line and the other port is at the battery input to the LPF. Therefore, the trace from LPF to the varactor and the lumped LPF elements are all taken in to account in the simulation. S_{11} and S_{21} determines antenna return loss and isolation between RF

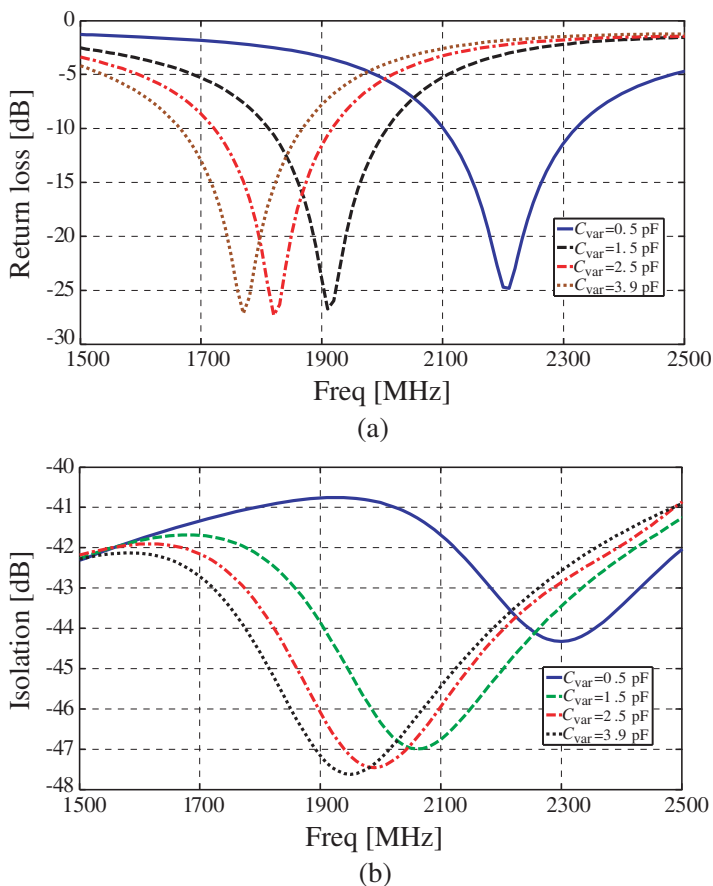


Figure 6. Two port simulation a varactor PIFA with a lump LPF DC bias: (a) return loss and (b) isolation.

feed-port to the DC bias point, respectively.

The simulation results of return losses and isolation are shown in Fig. 6 for several different varactor capacitances. One can observe the similarity between Fig. 2(a) and Fig. 6(a). It shows that adding the DC bias circuit including lumped LPF would not alter much the frequency tuning characteristics. The dynamic tuning range is almost identical (1.66~2.32 GHz here as compared to 1.69~2.32 GHz without the bias circuit). The isolation is also quite good, consistently below -40 dB over the entire frequency range of interest.

The prototype measurement results, accounting for the varactor and ceramic lump components parasitic effects are shown in Fig. 7.

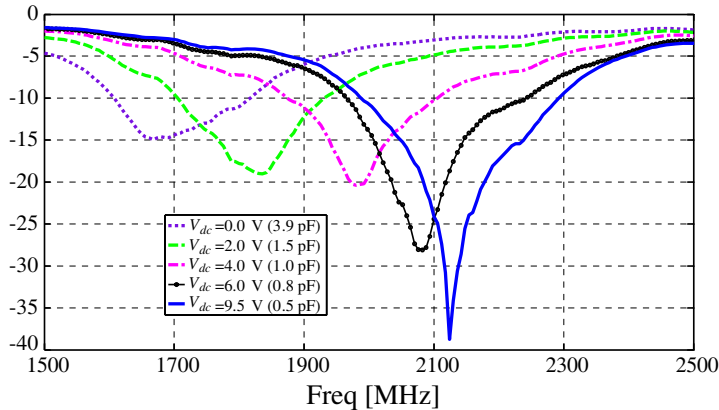


Figure 7. Measured return loss of varactor-loaded PIFA including dc bias circuits.

It is observed that the antenna dynamic tunable and width is from 1.61 to 2.29 GHz for DC voltage changing from 0 V to 9.5 V (C_{var} from 0.5 pF to 3.9 pF), which is very close to the theoretical prediction (1.66 to 2.32 GHz). This tunable varactor-loaded printed PIFA has about 34.8% relative bandwidth and 12% instant bandwidth. As comparing the simulation and measurement (Figs. 6(a) and 7), one can see the measured instant bandwidth at each bias voltage is shift down slightly from the simulation data. The main reason is that the capacitance versus bias voltage was calibrated at 1 MHz and is deviated slightly at 2 GHz band due to parasitics. Comparing Figs. 3 and 7, one can see that the varactor functions pretty much as expected and the bias circuits have a minor effect on the impedance matching.

Examples of measured radiation patterns are shown in Fig. 8. The patterns carry general features of a printed PIFA [26], more or less uniform radiation in the x - z plane (in front of the PIFA) and a deep null in the x - y plane (board surface). For each plane cut, there are patterns for three different bias voltages (three capacitor values). The radiation patterns by measurements are taken at 1.68 GHz for $C_{\text{var}} = 3.9$ pF (0 V), at 1.98 GHz for $C_{\text{var}} = 1.0$ pF (4 V), and at 2.12 GHz for $C_{\text{var}} = 0.5$ pF (9.5 V), respectively. In general, the gain pattern is not very sensitive to the varactor junction capacitance.

Antenna parameters based on both simulation and measurement for several bias voltages are shown in Table 2. Although the instant bandwidth compared very well, there is noticeable difference in the resonant frequency (the best impedance matching point). This is typically in antenna design, where the input impedance shifts due to

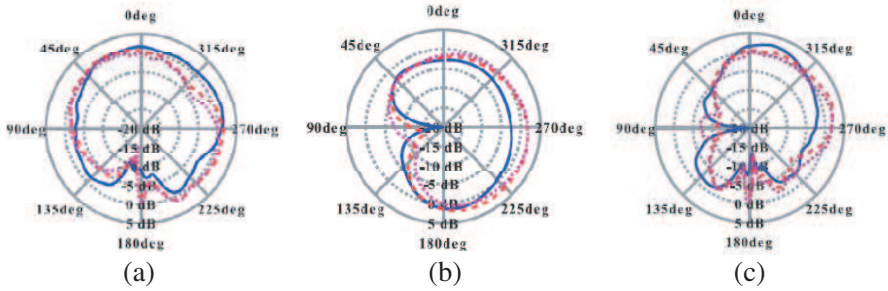


Figure 8. Measured PIFA gain patterns: (a) XZ plane, (b) XY plane, (c) YZ plane. (solid lines: 0.0 V, dashed lines: 4.0 V, and dotted lines: 9.5 V.)

Table 2. Simulated and measured antenna parameters of a tunable PIFA.

	Loading Cap. /Bias DC Voltage [pF]	Res. Freq [GHz]	Instant BW [%]	Max Gain [dB]	Efficiency [%]
Sim.	0.5	2.21	10.0	3.52	98.4
	1.5	1.91	10.5	2.65	93.8
	3.9	1.77	11.9	2.75	93.7
Meas.	3.9	1.68	12.3	2.57	66.8
	1.5	1.84	12.5	NA	NA
	0.5	2.12	14.0	2.43	70.4

the non-ideal fabrication process on circuit boards. Measured data show a slightly better instant bandwidth, but less gain and efficiency.

The best gain for each case occurs at the best matching condition (least return loss) and is around 2 to 3 dBi, a typical value for a printed PIFA. Antenna efficiency is related closely to the return loss. The best efficiency from measurement is around 70% to 80%, also consistent with a PIFA.

5. DOUBLE VARACTOR-LOADED STACKED INVERTED-F ANTENNAS

A double varactor-loaded PIFA structure is shown in Fig. 9 with its dimension parameters labeled. Two Panasonic MA27V19 silicon epitaxial SMT planar type variable capacitance diodes described in Table 3 are used.

The design is originated from the single-band reconfigurable PIFA in Fig. 1. Two of horizontal radiation arms are stacked on the PCB each with a shorting arm to control the impedance matching for the high- and low-bands. Hence, the longer horizontal arm on top is used to generate the 1st resonant radiation at the low-band, and will be termed as “up-arm”; the shorter horizontal arm in between up-arm and RF ground is used to generate the 2nd resonant radiation at the high-band, and will be termed as “down-arm”. The feeding arm of this antenna is shared by these two stacked radiation arms, and connected to the 50 Ohm microstrip line over the RF ground plane.

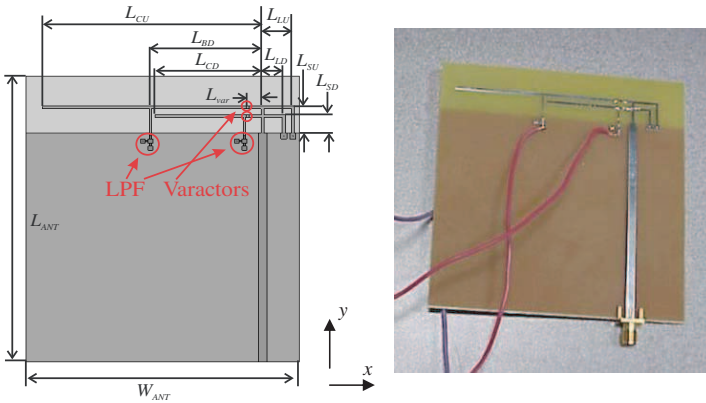
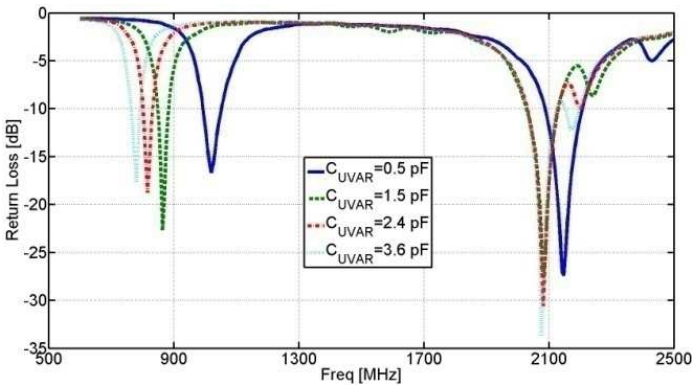


Figure 9. A double varactor-loaded PIFA with dual tunable bands.

In order to have antenna dynamic tunable frequency bandwidth covering both the high 1.7~2 GHz bands and low 0.8~1 GHz bands



(a)

Table 3. Measured antenna parameters of capacitor-loaded dual-band PIFA.

	Up / Down Loading Cap. [pF]	Res. Freq [GHz]	Max Gain [dB]	Efficiency [%]
Meas.	0.5 / 0.5	1.02	1.70	77.6
		2.16	3.05	62.7
	1.5 / 0.5	0.87	1.39	74.1
		2.08	2.66	57.1
	2.4 / 0.5	0.82	0.06	58.8
		2.08	2.36	57.3
	3.6 / 0.5	0.78	-0.04	57.3
		2.08	1.75	56.6
	0.5 / 1.5	0.98	2.02	79.7
		1.84	3.50	57.0
	0.5 / 2.4	0.94	1.38	72.1
		1.76	3.02	49.4
	0.5 / 3.6	0.94	1.32	73.7
		1.72	3.08	45.3

in 3G wireless systems, HFSS simulation is carried out to optimize the layout parameters. The resulting parameters are $L_{CU} = 72$ mm, $L_{CD} = 35$ mm, $L_{LU} = 10$ mm, $L_{LD} = 7$ mm, $L_{SU} = 9$ mm, and

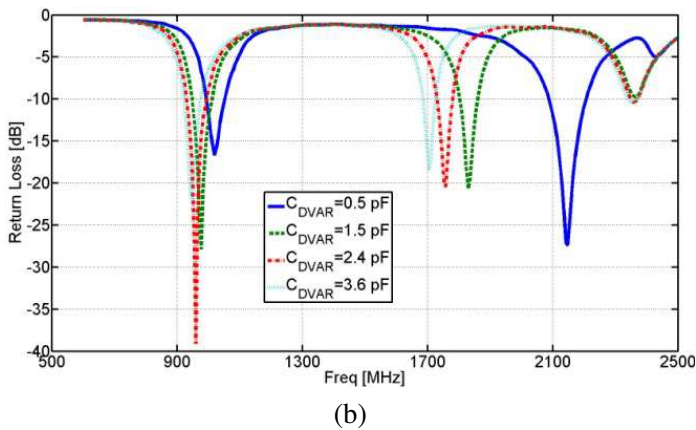


Figure 10. Measured return losses of capacitor-loaded dual-band PIFA: (a) for the lower band reconfiguration and (b) for the higher band reconfiguration.

$L_{SD} = 6$ mm. This antenna is fabricated on a conventional double-layer FR4 PCB 1.58 mm (62 mils) thick. The PCB size is 90 mm wide and 100 mm long, with 20 mm RF ground plane clearance opposite to the top antenna layer. Both of the up and down radiation arms are loaded with a varactor 5 mm away from the feeding arm (according to the results in Section 2). Thus, the higher band resonant frequency can be controlled by the down-arm varactor capacitance with a DC bias. Also, the lower resonant frequency is controlled by the up-arm varactor capacitance, with DC bias trace 31 mm away from the varactor ($L_{BD} = 31$ mm). Two T-type low-pass filter circuits are also designed at the tips of the DC bias traces for RF-DC isolation as described in the previous section. The antenna design is first investigated by HFSS full-wave simulations with directly loading lump capacitors on the up and down radiation arms. The antenna prototype was also fabricated and tested by the VNA for S -parameters and anechoic chamber for radiation patterns and efficiencies. This analysis also includes the low pass filter and bias circuit. Due to space limit, only measurement results in Fig. 10 are shown.

From the return-losses results, it is found that by varying the up-arm varactor capacitors from with 0.5 pF to with 3.6 pF (0 to 10 V DC bias), and keeping the down-arm capacitor (0 V bias) as of 0.5 pF in the measurements of antenna prototype, the 1st resonant frequency varies from 780 MHz to 1020 MHz, while the 2nd resonant frequency shifts from 2.14 GHz to 2.08 GHz (Fig. 10(a)). Hence, the dynamic tuning range for this case at the low-band is 19.7%, while the frequency shift at the high-band is less than 1.5%. Moreover, for the high-band tuning, while the up-arm loading capacitance remains unchanged at 0.5 pF but down-arm capacitance changes from 0.5 pF to 3.6 pF, the 2nd resonance of the antenna varies from 2.14 GHz to 1.70 GHz, and the 1st resonance just shifts from 948 MHz to 1.02 GHz, respectively (Fig. 10(b)). Thus, the dynamic tuning range for this case at high-band is 17.0%, while the frequency shift at low-band is less than 5.4%. Furthermore, the measured peak gain and efficiency at each resonant frequency are shown in Table 3.

In general, the HFSS simulations and prototype measurement results agree well and the discrepancies are within the anechoic chamber tolerance. The measured gain patterns for the three principal axes are shown in Figs. 11 and 12, for the low and high band operations, respectively. Each pattern is measured at the tuned frequency at each bias condition (4 different bias conditions with 4 different capacitances). It is observed that the variations of the antenna radiation patterns for each case corresponding to different loading capacitances are insignificantly at its own resonant frequency,

which is a desirable feature for many wireless terminal applications. In the lower operating band, the antenna is a fairly good uniform radiator. In the higher band, the antenna shows more directional radiation. The study shows that both the low and high operation bands of the antenna can be reconfigured by applying different loading capacitances separately. The antenna efficiencies within its own instant bandwidth are as high as over 55% at the lower band and over 45% at the higher band by measurements accounting for all parasitic losses. Also, the antenna maintains an acceptable maximum gain within its instant bandwidth and shows non-directional patterns on most of the azimuth planes. It is observed that both the antenna efficiencies and

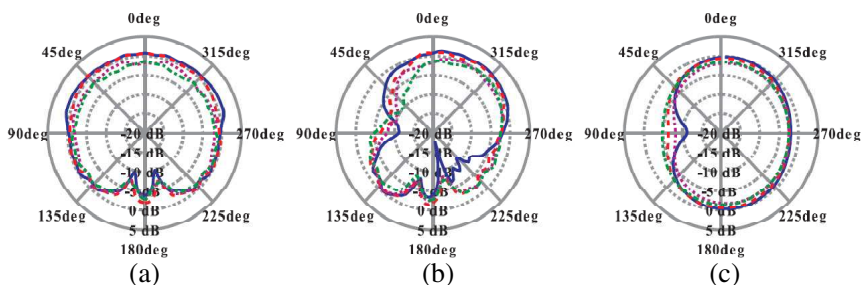


Figure 11. Measured gain patterns of varactor-loaded dual band PIFA for lower band reconfiguration: (a) XZ plane, (b) YZ plane, (c) XY plane. Solid lines: $C_{U\text{VAR}} = 0.5 \text{ pF}$, dashed lines: $C_{U\text{VAR}} = 1.5 \text{ pF}$, dotted lines: $C_{U\text{VAR}} = 2.4 \text{ pF}$, dashed-dotted lines: $C_{U\text{VAR}} = 3.6 \text{ pF}$.

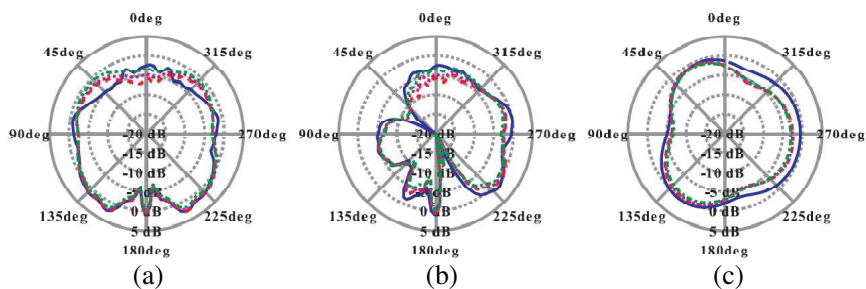


Figure 12. Measured gain patterns of varactor-loaded dual band PIFA for the higher band reconfiguration: (a) XZ plane, (b) YZ plane, (c) XY plane. Solid lines: $C_{U\text{VAR}} = 0.5 \text{ pF}$, dashed lines: $C_{U\text{VAR}} = 1.5 \text{ pF}$, dotted lines: $C_{U\text{VAR}} = 2.4 \text{ pF}$, dashed-dotted lines: $C_{U\text{VAR}} = 3.6 \text{ pF}$.

gains drop significantly outside the instant bandwidth. So the out-of-band interference rejection of this type of reconfigurable antennas is much stronger than the traditional multi-band antenna design and the narrow-bandwidth band-pass filter (BPF) at the radio front-end may not be necessary.

Isolation between DC bias circuit and RF port is investigated through HFSS simulation, where a 3-port model is used, with one for RF feeding port (port 1) and two for DC voltage bias. In general, it is found that when the LPF DC bias circuits for the two DC voltage ports are added, the differences of the return losses at the RF feed port for cases with or without DC bias traces added are insignificant. The parasitic radiation associated with the DC bias traces, hence, can be neglected. Also, the isolations between the RF feed-port and two DC bias ports are over 40 dB at all the frequencies of interest. The tuning varactors themselves are reverse biased, and thus can provide the DC isolations between two bias ports. Consequently, the individual tuning of the antenna 1st or 2nd resonance can be accomplished by changing the corresponding DC bias port voltage without much effect on the other resonance.

6. CONCLUSION

A tunable printed PIFA was proposed using a varactor at the radiation arm. A fixed capacitor PIFA was investigated first. It provided a feasibility study of capacitor tuned PIFA and served as a reference design for a varactor-loaded PIFA with bias circuits. The capacitor location closer to the feed line was found to provide a better tuning range. Based on both simulation and measurement, a good frequency tuning range (over 31%) from 1.69 GHz to 2.32 GHz was found, for capacitance less than 4 pF, a typical saturated value for RF varactors.

A lumped LPF was designed to provide better than 40 dB RF isolation between the antenna feed and the battery load. Panasonic MA27V19 varactor diode was implemented in the design with bias range 0~9.5 V and capacitance range 0.5 pF to 3.9 pF. A varactor printed PIFA together and the bias circuits was designed (with HFSS simulation), fabricated, and tested. The results showed good agreement. Measurement showed 1.62 GHz to 2.29 GHz tuning range with an instant bandwidth about 12% and a dynamic bandwidth over 30%. The gain 2~3 dBi and efficiency (70~80%) are similar to a regular PIFA. The parasitic and resistive effect of the varactor and lumped elements in LPF were found insignificant.

A dual band two-arm printed PIFA was also proposed with two varactors loaded at the each of the radiating arm. Both varactors

could be biased simultaneously and the operating frequency could be reconfigured to any of the 3G band (800–900 MHz and 1.8–2.0 GHz). The dynamic tuning range for the low-band is 19.7%, while the frequency shift at the high-band is less than 1.5%. The dynamic tuning range for the high-band is 17.0%, while the frequency shift at low-band is less than 5.4%. The in-band maximum gain is around 1-3 dB though out the 3G spectrum.

REFERENCES

1. Waterhouse, R. and N. Shuley, "Full characterization of varactor-loaded, probe-fed, rectangular, microstrip patch antennas," *IEE Proceedings, Microwaves, Antennas and Propagation*, Vol. 141, No. 5, 367–373, 1994.
2. Yang, F. and Y. Rahmat-Samii, "Patch antenna with switchable slot (PASS): Dual-frequency operation," *Microwave and Optical Technology Letters*, Vol. 31, No. 3, 165–168, 2001.
3. Nikolaou, S., R. Bairavasubramanian, C. Lugo, I. Carrasquillo, D. C. Thompson, G. E. Ponchak, J. Papapolymerou, and M. M. Tentzeris, "Pattern and frequency reconfigurable annular slot antenna using PIN diodes," *IEEE Transactions on Antennas and Propagation*, Vol. 54, No. 2, 439–448, 2006.
4. Brown, E., "RF-MEMS switches for reconfigurable integrated circuits," *IEEE Transactions on Microwave Theory and Techniques*, Vol. 46, No. 11, 1868–1880, 1998.
5. Rebeiz, G. M., *RF MEMS: Theory, Design, and Technology*, Wiley, New York, 2003.
6. Anagnostou, D., G. Zheng, M. Chryssomallis, J. Lyke, G. Ponchak, J. Papapolymerou, and C. Christodoulou, "Design, fabrication, and measurements of an RF-MEMS-based self-similar reconfigurable antenna," *IEEE Transactions on Antennas and Propagation*, Vol. 54, No. 2, 422–432, 2006.
7. Cetiner, B., H. Jafarkhani, J.-Y. Qian, H. J. Yoo, A. Grau, and F. De Flaviis, "Multifunctional reconfigurable MEMS integrated antennas for adaptive MIMO systems," *IEEE Communications Magazine*, Vol. 42, No. 12, 62–70, 2004.
8. Al-Dahleh, R., C. Shafai, and L. Shafai, "Frequency-agile microstrip patch antenna using a reconfigurable MEMS ground plane," *Microwave and Optical Technology Letters*, Vol. 43, No. 1, 64–67, 2004.
9. Jung, C. W., M. J. Lee, G. P. Li, and F. De Flaviis, "Reconfigurable scan-beam single-arm spiral antenna integrated

- with RF-MEMS switches," *IEEE Transactions on Antennas and Propagation*, Vol. 54, No. 2, 455–463, February 2006.
10. Kolsrud, A., M.-Y. Li, and K. Chang, "Dual-frequency electronically tunable CPW-fed CPS dipole antenna," *Electronics Letters*, Vol. 34, No. 7, 609–611, 1998.
 11. Behdad, N. and K. Sarabandi, "Dual-band reconfigurable antenna with a very wide tuning range," *IEEE Transactions on Antennas and Propagation*, Vol. 54, No. 2, 409–416, February 2006.
 12. Aberle, J., S.-H. Oh, D. Auckland, and S. Rogers, "Reconfigurable antennas for wireless devices," *IEEE Antennas and Propagation Magazine*, Vol. 45, No. 6, 148–154, 2003.
 13. Guo, Y.-X., M. Y. W. Chia, and Z. N. Chen, "Miniature built-in multiband antennas for mobile handsets," *IEEE Transactions on Antennas and Propagation*, Vol. 52, No. 8, 1936–1944, August 2004.
 14. Guo, Y.-X. and H. S. Tian, "New compact six-band internal antenna," *IEEE Antennas and Wireless Propag. Lett.*, Vol. 3, No. 1, 295–297, 2004.
 15. Karmakar, N. C. and M. E. Bialkowski, "High performance switches using low cost diodes at L-band," *Microwave and Optical Technology Letters*, 367–370, March 2002.
 16. Behdad, N. and K. Sarabandi, "A varactor-tuned dual-band slot antenna," *IEEE Transactions on Antennas and Propagation*, Vol. 54, No. 2, 401–408, 2006.
 17. Rowell, C. R. and R. D. Murch, "A capacitively loaded PIFA for compact mobile telephone handsets," *IEEE Transactions on Antennas and Propagation*, Vol. 45, 837–842, May 1997.
 18. Song, C. T., P. S. Hall, H. G. Shiraz, and D. Wake, "Triple band planar inverted-F antennas for handheld devices," *Electronics Letters*, Vol. 36, 112–114, January 2000.
 19. Karmakar, N., "Shorting strap tunable stacked patch PIFA," *IEEE Transactions on Antennas and Propagation*, Vol. 52, No. 11, 2877–2884, 2004.
 20. Panayi, P., M. Al-Nuaimi, and I. Ivriissimtzis, "Tuning techniques for planar inverted-F antenna," *Electronics Letters*, Vol. 37, No. 16, 1003–1004, 2001.
 21. Panaia, P., C. Luxey, G. Jacquemod, R. Staraj, L. Petit, and L. Dussopt, "Multistandard reconfigurable PIFA antenna," *Microwave and Optical Technology Letters*, Vol. 48, No. 10, 1975–1977, October 2006.
 22. Boyle, K. R. and L. P. Ligthart, "Radiating and balanced mode

- analysis of PIFA antennas,” *IEEE Transactions on Antennas and Propagation*, Vol. 54, No. 1, 231–237, January 2006.
23. Boyle, K. R. and P. J. Massey, “Nine-band antenna system for mobile phones,” *Electronics Letters*, Vol. 42, No. 5, 265–266, March 2006.
 24. Boyle, K. R., Y. Yuan, and L. P. Ligthart, “Analysis of mobile phone antenna impedance variations with user proximity,” *IEEE Transactions on Antennas and Propagation*, Vol. 55, No. 2, 364–372, February 2007.
 25. Boyle, K. R. and P. G. Steeneken, “A five-band reconfigurable PIFA for mobile phones,” *IEEE Transactions on Antennas and Propagation*, Vol. 55, No. 11, 3300–3309, November 2007.
 26. Soras, C., M. Karaboikis, G. Tsachtsiris, and V. Makios, “Analysis and design of an inverted-F antenna printed on a PCMCIA card for the 2.4 GHz ISM band,” *IEEE Antennas and Propagation Magazine*, Vol. 44, No. 1, 37–44, February 2002.
 27. Matsushita Electric Industrial Co. Ltd., “Panasonic MA27V19 silicon epitaxial planar type variable capacitance diodes data sheet,” July 2002.
 28. Liang, J., “Frequency reconfigurability analysis of electrically small antenna,” Ph.D. Dissertation, University of Illinois at Chicago, June 2008.